

Galactic HCO^+ Absorption toward Compact Extragalactic Radio Sources

Geumsook Park^{†,1,2} • Bon-Chul Koo² •
Kee-Tae Kim¹ • Do-Young Byun^{1,3,4} •
Carl E. Heiles⁵

Abstract As part of the search for the “dark molecular gas (DMG),” we report on the results of HCO^+ $J = 1 - 0$ absorption observations toward nine bright extragalactic millimeter wave continuum sources. The extragalactic sources are at high Galactic latitudes ($|b| > 10^\circ$) and seen at small extinction ($E(B-V) \lesssim 0.1$ mag). We have detected the HCO^+ absorption lines toward two sources, B0838+133 and B2251+158. The absorption toward B2251+158 was previously reported, while the absorption toward B0838+133 is a new detection. We derive hydrogen column densities or their upper limits toward the nine sources from our observations and compare them to those expected from CO line emission and far-infrared dust continuum emission. Toward the seven sources with no HCO^+ detection, CO emission has not been detected, either. Thus the sight lines are likely to be filled with almost pure atomic gas. Toward the two sources with HCO^+ detection, CO emission has been also detected. Comparison of the H_2 column densities from HCO^+ absorption and CO emission suggests a non-negligible amount of DMG toward B0838+133.

Keywords ISM: clouds – radio lines: ISM

1 Introduction

The Interstellar Medium (ISM) is mainly composed of hydrogen in three phases: atomic (H I), molecular (H_2), and ionized (H II). H I atoms are directly observed in the H I 21-cm line, while most H_2 molecules are in so cold states that they cannot be excited by any radiative transition. Instead, carbon monoxide (CO) molecular lines are usually used to trace H_2 . That is, the amount of CO emission has been used to infer that of molecular gas, which is almost entirely composed of H_2 , by using an empirical CO- H_2 conversion factor. Recently, however, researchers have discovered “dark gas,” invisible in H I and CO, in the solar neighborhood; this “dark gas” has a non-negligible mass. It can be found by excess γ ray emission (e.g., Grenier et al. 2005; Abdo et al. 2010) or excess dust emission (e.g., Planck Collaboration et al. 2011a,b). These observational results imply there is an additional ISM component that cannot be traced by H I or CO line observations. The “dark gas” component is generally considered to be a molecular gas, a so-called “dark molecular gas (DMG)” (e.g., Lucas and Liszt 1996), despite another suggestion by Fukui et al. (2014, 2015) that optically thick and cold H I gas mainly contributes “dark gas.”

Theoretically, the presence of DMG is supported by the photodissociation region (PDR) model (e.g., van Dishoeck and Black 1988; Wolfire et al. 2010). The PDR model predicts an intermediate layer between H I-to- H_2 and H_2 -to-CO transitions, where CO cannot survive UV photodissociation but H_2 can self-shield. Wolfire et al. (2010) inferred that the H I-to- H_2 transition is located at a visual extinction of

Geumsook Park

Bon-Chul Koo

Kee-Tae Kim

Do-Young Byun

Carl E. Heiles

¹Korea Astronomy and Space Science Institute, Daedeokdae-ro, Yuseong-gu, Daejeon 34055, Republic of Korea

²Department of Physics and Astronomy, Seoul National University, 1 Gwanak-ro, Gwanak-gu, Seoul 08826, Republic of Korea

³Korea University of Science and Technology, 217 Gajeong-ro, Yuseong-gu, Daejeon 34113, Republic of Korea

⁴Yonsei University, Yonsei-ro 50, Seodaemun-gu, Seoul 03722, Republic of Korea

⁵Radio Astronomy Lab, UC Berkeley 601 Campbell Hall, Berkeley, CA 94720, USA

[†]pgs@kasi.re.kr

$A_V \simeq 0.2$ mag, which is consistent with observational findings; for example, Paradis et al. (2012) and Planck Collaboration et al. (2011a) found the threshold to be 0.2 mag and 0.4 mag, respectively. Corresponding reddenings $E(B-V)$ are 0.065 and 0.13 mag, respectively, assuming that $A_V/E(B-V) = 3.1$ for the diffuse ISM (Savage and Mathis 1979). The main chemical route associated with CO in diffuse clouds predicts that OH, C^+ , and HCO^+ can be observable before CO formation (van Dishoeck and Black 1988). Such elements or molecules would be useful tracers for CO-dark molecular gas. Liszt and Lucas (1996) and Lucas and Liszt (1996) confirmed that OH and HCO^+ do reliably trace DMG. Tang et al. (2017) also showed that C^+ could be a useful tracer for DMG.

Lucas and Liszt (1996, hereafter, LL96) surveyed HCO^+ absorption toward thirty lines-of-sight (LOSs) of extragalactic background continuum sources, finding detectable absorption lines for eighteen sources. Since then, there have been several studies of HCO^+ absorption lines (Liszt and Lucas 2000; Liszt et al. 2010, and see a compilation in Appendix E of Liszt et al. (2010)). In this paper, using the Korean VLBI Network (KVN) 21 m telescope in the single dish mode, we present the observational results of HCO^+ absorption lines toward several background sources missing before. In Sections 2 and 3, we describe our KVN observations and results, respectively. In Section 4, we discuss gas properties of the individual LOSs. Section 5 summarizes the paper.

2 Observations

Using the KVN 21-m telescope at the Yonsei station in the single dish mode, we observed nine positions in the transition $J = 1-0$ of HCO^+ (89.188526 GHz) (Kim et al. 2011; Lee et al. 2011). The positions lie on a background of extragalactic compact radio sources (such as quasars or AGN), which are listed in Table 1; our intent was to observe absorption lines from Galactic dark molecular gas in the foreground. The observations toward B0838+133 and B2251+158 were performed on 07 February 2013, and the others during the period from September 2014 to January 2015. The digital spectrometer was set to have 4096 channels with a bandwidth of 64 MHz (~ 216 km s $^{-1}$ at 89 GHz) and centered at $v_{LSR} = 0$ km s $^{-1}$.¹ A single channel width is 0.016 MHz, giving a velocity resolution of 0.05 km s $^{-1}$. The 21-m telescope had a main beam

efficiency of $\sim 36\%$ and a beam size (Full Width at Half Maximum; FWHM) of $31''$ at 89 GHz. Observations were done in dual polarization mode. While data for B0838+133 and B2251+158 were taken by position switching (PS), the other data were obtained by frequency switching (FS). For the off-position of the PS mode, four locations, $(-1', -1')$, $(+1', -1')$, $(-1', +1')$, and $(+1', +1')$ from the on-position, were alternately observed. For the FS mode, the frequency offset was set to 16 MHz. Pointing observations were usually performed approximately once every hour (~ 2.5 hours at the longest). We used only data having system temperature (T_{sys}) less than 400 K. Total exposure time (t_{tot}) of the data that were utilized finally are noted in the seventh column of Table 1. Seven sources were missed in previous surveys, while two sources, B0316+413 and B2251+158, were observed in LL96.

When planning observations, the background galaxies in Table 1 were selected as bright radio continuum sources mostly with flux densities > 3 Jy around the observing frequency, but about half had lower values or were even invisible during our observing period because of their flux variability. The flux densities are listed in the second column of Table 2. Flux measurements are performed with Gaussian fittings of average ‘‘cross-scan’’ data obtained during our KVN observations. There was no cross-scan data for B0838+133, so we assumed its flux based on data from the nearest dates in the ALMA calibrator database. For B2249+185, most of the observing dates had no signal. B2249+185 may have been invisible during the observing season, which implies that the source may have been radio-quiet during those days.

3 Results

Figs. 1 and 2 show the spectra observed for the HCO^+ -detected and -undetected sources, respectively. For the HCO^+ spectra, Hanning smoothing is applied once or twice using ‘CLASS’ from the GILDAS software package². Then, each spectrum is baseline-corrected by n th-order polynomial fitting: third and first for B0838+133 and B2251+158, respectively, and seventh (or fifth) for the others. The spectral velocity range shown in Fig. 2 is based on where the Galactic H I emission of the Leiden/Argentine/Bonn (LAB) all-sky survey data (0 $^{\circ}$ 5-pixel with an angular resolution of $\sim 36'$; Kalberla et al. 2005) is seen in the same LOS; the H I line profiles toward our nine LOSs are displayed together in Figs. 1 and 2. The resulting root-mean-square

¹ Velocities (v_{LSR}) in this paper is with respect to the local standard of rest (LSR).

²<http://www.iram.fr/IRAMFR/GILDAS>

Table 1 Target Sources with Observational Log

Name	Other Name	α_{2000} (h:m:s)	δ_{2000} (d:m:s)	ℓ ($^{\circ}$)	b ($^{\circ}$)	t_{tot} (min)	$T_{A^*,\text{RMS}}$ (mK)	Observing Dates (YYMMDD)
(1)	(2)	(3)	(4)	(5)	(6)	(7)	(8)	(9)
B0316+413	3C84	03:19:48.16	+41:30:42.1	150.576	-13.261	345	7	141007, 141011, 141201, 150104
B0420-014	PKS 0420-01	04:23:15.80	-01:20:33.1	195.290	-33.140	234	7	141201
B0838+133	3C207	08:40:47.59	+13:12:23.6	212.968	+30.139	88	10	130207
B0851+202	OJ287	08:54:48.88	+20:06:30.6	206.812	+35.821	398	7	141007, 141009, 141011, 141201
B1228+126	VIRGO A, NGC 4486	12:30:49.42	+12:23:28.0	283.778	+74.491	300	7	141109, 141116, 141201, 150104
B1633+382	4C38.41	16:35:15.49	+38:08:04.5	61.086	+42.337	435	7	140930, 141007, 141109, 141116, 141201, 150104
B2223-052	3C446	22:25:47.26	-04:57:01.4	58.960	-48.843	250	7	141109, 141116, 141201, 150104
B2249+185	3C454	22:51:34.74	+18:48:40.1	87.354	-35.648	283	8	141009, 141011, 141109, 150104
B2251+158	3C454.3	22:53:57.75	+16:08:53.6	86.111	-38.184	52	13	130207

Note: Columns are as follows: (1) IAU B1950.0 source name; (2) source name in other catalogs; (3)–(6) source coordinates; (7) total integration time with $T_{\text{sys}} < 400$ K; (8) RMS noise level on the T_{A^*} scale at a velocity resolution of 0.1 km s^{-1} ; (9) Observing dates (2-digit year to be interpreted as 20xx)

Table 2 HCO^+ Absorption Line Parameters toward Nine Sources

Name	$S_{86 \text{ GHz}}^a$ (Jy)	v_0 (km s^{-1})	Δv_{FWHM} (km s^{-1})	τ_0	$\int \tau dv$ (km s^{-1})	$N(\text{HCO}^+)$ (10^{12} cm^{-2})
B0316+413	19.0 \pm 0.3	< 0.02	< 0.02	< 0.02
B0420-014	1.2 \pm 0.1	< 0.28	< 0.30	< 0.33
B0838+133	~ 0.7	+4.44 \pm 0.04	0.47 \pm 0.09	1.44 \pm 0.23	0.72 \pm 0.18	0.81 \pm 0.20
B0851+202	4.0 \pm 0.1	< 0.09	< 0.10	< 0.11
B1228+126	4.5 \pm 0.1	< 0.08	< 0.09	< 0.10
B1633+382	1.7 \pm 0.1	< 0.21	< 0.22	< 0.25
B2223-052	0.9 \pm 0.1	< 0.42	< 0.45	< 0.50
B2249+185	< 0.3
B2251+158	5.0 \pm 0.1	-9.47 \pm 0.09	0.92 \pm 0.24	0.22 \pm 0.03	0.22 \pm 0.06	0.24 \pm 0.07
		-10.84 \pm 0.33	1.27 \pm 0.63	0.07 \pm 0.02	0.09 \pm 0.06	0.11 \pm 0.06

^aThe flux densities of the background sources except B0838+133 were measured using the KVN 21-m telescope during our observation period. The conversion factor from T_{A^*} to flux density is $\sim 16 \text{ Jy K}^{-1}$. The 86 GHz flux of B0838+133 assumes 0.7 Jy, which includes one valid decimal place, based on a known database: 0.73 Jy at 91.5 GHz on 2013-12-29 in the ALMA calibrator database (<https://almascience.eso.org/sc/>).

(RMS) antenna temperature values at a velocity resolution of 0.1 km s^{-1} are listed in the last column of Table 1; typical RMS noise level (1σ) is 6 mK. We detected an HCO^+ absorption line in two sources: the existence of an HCO^+ absorption line in the LOS of B2251+158 has already been reported by LL96, while we detected for the first time an absorption feature toward B0838+133. However, none of the other samples show any absorption lines. Interestingly, a weak blue wing is seen in the HCO^+ line of B2251+158, as noted in Liszt and Pety (2012).

For the two detected cases, we applied a Gaussian fit with an assumption of a single component for B0838+133 and two components for B2251+158. This was done because the latter's profile shows one more negative-velocity component that is weak but likely real; this component also appears in profiles from previous observations (LL96; Liszt and Lucas 2000; Liszt and Pety 2012). Table 2 presents the resultant parameters for the central velocity (v_0), velocity width

(Δv_{FWHM}), optical depth (τ) at v_0 , and integrated optical depth. Uncertainties of the first three parameters were taken from those derived during Gaussian fit (GAUSSFIT in IDL); the last one was from the results of Monte Carlo simulations using imaginary profiles formed from observed spectra with 1σ RMS noise. For the undetected cases, except for B2249+185, we give an upper limit assuming one Gaussian component with peak temperature of $3 \times T_{A^*,\text{RMS}}$ and a line width of 1 km s^{-1} . For reference, the mean HCO^+ line width of detected sources in LL96 is 0.95 km s^{-1} . Our results are consistent with the results of LL96 for B0316+413 and B2251+158. For B2251+158, HCO^+ profiles were reported in Liszt and Lucas (2000) as well as LL96, and they gave results of single-component Gaussian fit, which is consistent with the total optical depth of our two components within 1σ uncertainty. As shown in the last column in Table 2, we derived the HCO^+ column density, $N(\text{HCO}^+)$, using the relationship with the integrated HCO^+ optical depth (e.g., see Liszt et al. 2010),

Fig. 1 Left: HCO^+ absorption line profiles toward B0838+133 and B2251+158. Hanning smoothing was applied twice, resulting in a velocity resolution of 0.2 km s^{-1} . The vertical dotted line marks the adjacent H I peak velocity at which HCO^+ absorption line is detected. Right: H I line profile toward the two sources. The profiles are from the LAB survey (FWHM = $30'$) at Galactic coordinates written at the upper left corner of each panel. The vertical dotted line marks where HCO^+ absorption line is detected.

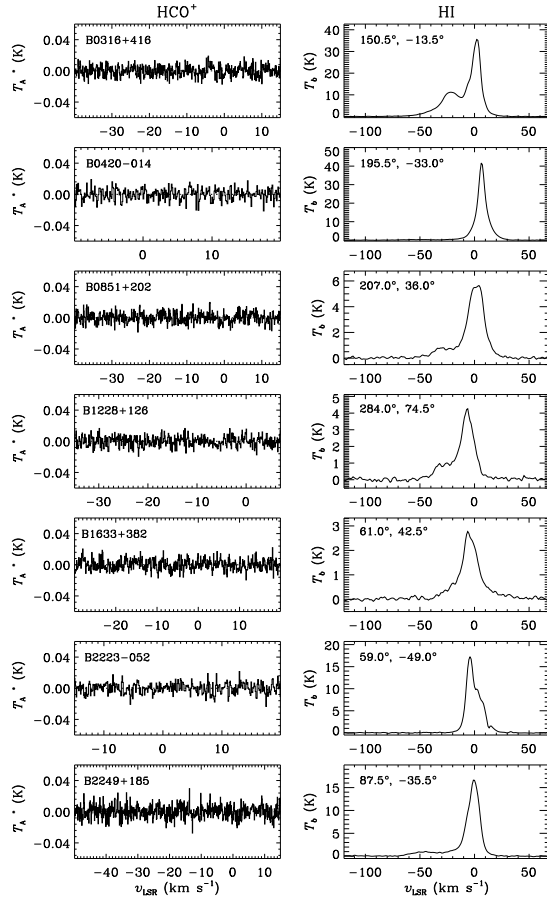
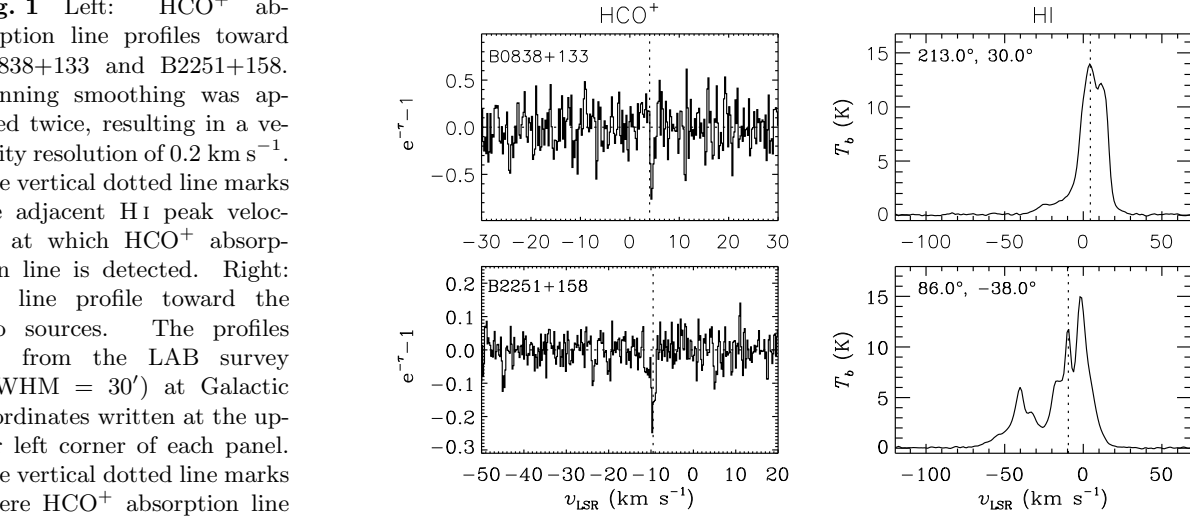


Fig. 2 Same as Figure 1 but for HCO^+ -undetected sources.

i.e.,

$$N(\text{HCO}^+) = 1.12 \times 10^{12} \text{ cm}^{-2} \int \tau_{\text{HCO}^+} dv \text{ (km s}^{-1}\text{)}^{-1}.$$

4 Discussion

We wondered if there is “dark gas” indeed toward the HCO^+ -detected LOSs or no dark gas toward the undetected LOSs. To answer this question, we consider the total column density of hydrogen nuclei, $N(\text{H})$, in the LOS. $N(\text{H})$ can be determined by the sum of column densities of H I and H_2 , i.e., $N(\text{H}) = N(\text{H I}) + 2N(\text{H}_2)$, ignoring the ionized gas. Alternatively, it can be inferred using the relation with optical reddening $E(B - V)$. Since these two methods are independent, we can discuss the implications of our observational results by comparison between measurements of the two approaches.

4.1 $N(\text{H I})$ and $N(\text{H}_2)$ derived from radio tracers

As mentioned in Section 1, $N(\text{H I})$ is obtained directly by H I 21-cm line observations, while $N(\text{H}_2)$ is usually inferred from integrated CO intensity (W_{CO}) using the empirical relationship between $N(\text{H}_2)$ and W_{CO} . That is, $N(\text{H I})$ is calculated using the equation of

$$N(\text{H I})/W_{\text{H I}} = 1.82 \times 10^{18} \text{ cm}^{-2} \text{ (K km s}^{-1}\text{)}^{-1}, \quad (2)$$

where $W_{\text{H I}} = \int T_{\text{b, H I}} dv$, and with an assumption of optically thin conditions, and $N(\text{H}_2)$ is derived from

$$N(\text{H}_2)/W_{\text{CO}} = 2.0 \times 10^{20} \text{ H}_2 \text{ cm}^{-2} \text{ (K km s}^{-1}\text{)}^{-1} \quad (3)$$

with $\pm 30\%$ uncertainty (Bolatto et al. 2013). As another approach, $N(\text{H}_2)$ can be measured using the relation with $N(\text{HCO}^+)$ (e.g., LL96; Liszt et al. 2010), i.e.,

$$N(\text{HCO}^+)/N(\text{H}_2) = 3 \times 10^{-9}. \quad (4)$$

For W_{HI} , we obtained a line profile at a given position from the LAB data (see Figs. 1 and 2) and integrated it over LSR velocities of $\pm 150 \text{ km s}^{-1}$ wide enough to contain most Galactic H I gas. Moreover, W_{CO} values were taken from the literature of Liszt and Wilson (1993), Liszt et al. (2010), and Li et al. (2018). Table 3 lists the values of W_{HI} and W_{CO} that we adopted. In the 2nd-4th columns of Table 4 we list the H I and H_2 column densities derived using equations (2)–(4); the sums of different H_2 measurements are in the 5th-6th columns. CO line emission was detected toward the two sources of B0838+133 and B2251+158, but not in the others except B1228+126, which has no available literature data. CO emission toward B0838+133 was not detected in the previous survey of Liszt (1994), but was detected in a recent deeper survey of Li et al. (2018). Although CO emission is observed toward both HCO^+ -detected sources, W_{CO} of B2251+158 is about two times larger than that of B0838+133. For B0838+133, the HCO^+ absorption line is decomposed as a single component at a velocity similar to that of the CO emission line (Li et al. 2018), but $N(\text{H}_2)$ derived from HCO^+ is three times larger than $N(\text{H}_2)$ inferred from CO. The given $N(\text{HCO}^+)$ value that was used for $N(\text{H}_2)$ is uncertain, but it may still be possible that molecular gas not traced by CO exists toward B0838+133.

Table 3 H I and CO Line Intensities and $E(\text{B}-\text{V})$ toward Nine Sources

Name	W_{HI}^1 (K km s $^{-1}$)	W_{CO}^2 (K km s $^{-1}$)	$E(\text{B}-\text{V})^3$ (mag)
B0316+413	710.72	<0.20	0.14
B0420-014	469.05	<0.52	0.11
B0838+133	289.62	0.43 ± 0.07	0.08
B0851+202	129.86	<0.52	0.02
B1228+126	87.82	...	0.02
B1663+382	61.79	<0.52	0.01
B2223-052	241.85	<0.52	0.06
B2249+185	273.70	...	0.05
B2251+158	381.29	0.91 ± 0.04	0.09

¹Integrated H I intensity (W_{HI}) obtained from the LAB data.

²Integrated CO intensity (W_{CO}) obtained from previous studies (Liszt and Wilson 1993; Liszt et al. 2010; Li et al. 2018). See Appendix for details.

³Total reddening ($E(\text{B}-\text{V})$) from Schlafly and Finkbeiner (2011).

4.2 $N(\text{H})$ derived from $E(\text{B}-\text{V})$

$E(\text{B}-\text{V})$ toward each source is obtained from the database of Schlafly and Finkbeiner (2011) which originates from the work of Schlegel et al. (1998). Schlegel et al. (1998) derived $E(\text{B}-\text{V})$ from far-infrared dust emission at 2'.5-pixels with an angular resolution of 6' and a measurement error of 16%. After that, Schlafly and Finkbeiner (2011) re-examined the values of Schlegel et al. (1998) and provided new estimates, which are somewhat lower (14% downward) than the original data. We finally picked the mean value of Schlafly and Finkbeiner (2011) for a 5'-radius circle, with each center provided on the webpage³. (See the values listed in the last column of Table 3.) A canonical conversion factor of the dust-to-gas ratio is $5.8 \times 10^{21} \text{ H (cm}^{-2}/\text{mag)}$ (Savage et al. 1977; Bohlin et al. 1978). Recently, however, Liszt (2014) examined the relationship between $E(\text{B}-\text{V})$ and $N(\text{HI})$ using H I measurements at high latitudes ($|b| \gtrsim 20^\circ$), where neutral atomic gas is very likely to predominate. Liszt (2014) found that the conversion factor should be higher at $E(\text{B}-\text{V}) \lesssim 0.1 \text{ mag}$. It is $8.3 \times 10^{21} \text{ H (cm}^{-2}/\text{mag)}$. Since they used the pre-update $E(\text{B}-\text{V})$ data of Schlegel et al. (1998), we divide by 0.86 to adjust the factor and obtain the equation of

$$N(\text{H})/E(\text{B}-\text{V}) = 9.65 \times 10^{21} \text{ H (cm}^{-2}/\text{mag)} \\ \text{for } E(\text{B}-\text{V}) \lesssim 0.1 \text{ mag.} \quad (5)$$

Most LOSs have $E(\text{B}-\text{V}) < 0.1 \text{ mag}$, while toward B0316+413 and B0420-014 are $E(\text{B}-\text{V}) = 0.14$ and 0.11 mag , respectively. We adopted the equation (5) for our all sources and obtained values of $N(\text{H})$ written in the last column of Table 4.

Comparing between our HCO^+ observational results and $E(\text{B}-\text{V})$, it is interesting that HCO^+ has not been detected toward B0316+413 and B0420-014 although their $E(\text{B}-\text{V})$ values are relatively high ($> 0.1 \text{ mag}$) compared to the HCO^+ -detected sources. We also note that their $E(\text{B}-\text{V})$ values are lower or comparable to the threshold of Planck Collaboration et al. (2011a) which is mentioned in Section 1. So far, HCO^+ absorption observations toward 31 LOSs (not counting B2249+185) at $|b| > 10^\circ$ were made by this work and previous studies (LL96; Liszt and Lucas 2000; Liszt et al. 2010, See Appendix for the compiled dataset.), and a total of four LOSs (including B1908-201 and B1749+096) are in such a case and also have no CO emission. If the LOSs have no Galactic molecular gas even DMG, is there a possibility of an additional source, such as high-velocity clouds (HVCs), increasing $E(\text{B}-\text{V})$? We checked works of literature and also an H I line profile of LAB data, there seems no HVC toward all LOSs except B1749+096. H I gas at high velocities

Table 4 Column Densities of Hydrogen Atomic and Molecular Gas

Tracer Source	H I	H ₂		Total H (H I + 2H ₂)		
	H I	CO	HCO ⁺	H I & CO	H I & HCO ⁺	E(B−V)
B0316+413	12.9	< 0.4	< 0.08	< 13.7	< 13.1	13.5
B0420−014	8.5	< 1.0	< 1.1	< 10.5	< 10.7	10.6
B0838+133	5.3	0.9	2.7	7.1	10.7	7.7
B0851+202	2.4	< 1.0	< 0.4	< 4.4	< 3.2	1.9
B1228+126	1.6	...	< 0.3	...	< 2.2	1.9
B1663+382	1.1	< 1.0	< 0.8	< 3.1	< 2.7	1.0
B2223−052	4.4	< 1.0	< 1.7	< 6.4	< 7.8	5.8
B2249+185	5.0	4.8
B2251+158	6.9	1.8	1.2	10.5	9.3	8.7

Note: Column densities in 10^{20} (cm^{-2}). For the detail description of table entries, see Section 4.

($v_{\text{LSR}} \sim 112 - 140 \text{ km s}^{-1}$) in the LOS of B1749+096 was reported in Lockman et al. (2002) and suggested to be associated with HVC Complex C. However, the presence of dust in Complex C is controversial (e.g., Miville-Deschênes et al. 2005; Peek et al. 2009).

4.3 Comprehensive analysis

Most HCO⁺-undetected sources do not show CO emission, either. Their values of $N(\text{HI})$ and $N(\text{H})$ from $E(\text{B} - \text{V})$ seem to be consistent, which suggests that such LOSs are mainly filled with purely atomic gas. The first panel of Fig. 3 shows a diagram comparing the H I column densities with total reddening. The data observed in the LOSs at high latitudes ($|b| > 10^\circ$), listed in Table E1 of Liszt et al. (2010) as well as this paper, are used (See Appendix). Their column densities are derived using the same ways in this paper. Green diamonds indicate the LOSs in which neither HCO⁺ nor CO are seen. Such sources are well located near a dashed line which is drawn using a higher conversion factor of $N(\text{H})/E(\text{B} - \text{V})$ than a conventional one (See Section 4.2). It may be hard to constrain the threshold $E(\text{B} - \text{V})$ value of the H I-to-H₂ transition from our results, but at least any source with $E(\text{B} - \text{V}) \lesssim 0.06$ mag might not be DMG. This result agrees well with the estimate of Liszt (2014), $E(\text{B} - \text{V}) \lesssim 0.07$ mag (The original value of $E(\text{B} - \text{V})$ has been corrected because of the same reason mentioned in Section 4.2.).

According to the previous studies (e.g., LL96; Liszt and Pety 2012), most of HCO⁺-detections are within $b \simeq \pm 15^\circ$, so the non-detection results from our observations (all except one at $|b| > 30^\circ$) are not very surprising. On the other hand, considering this work and previous studies together, six LOSs at $|b| > 15^\circ$ showed HCO⁺-detection. Half of them, how-

ever, show CO-detection: B0838+133, B2251+158, and B0954+658 ($l, b = 145.746^\circ, +43.132^\circ$).

Fig. 3b compares $N(\text{H}_2)$ obtained from the two H₂ tracers of HCO⁺ and CO. At $N(\text{H}_2) < 10^{21} \text{ cm}^{-2}$, all HCO⁺-detected sources except B2251+158 have higher values of $N(\text{H}_2)$ from HCO⁺ than those from CO. Figs. 3c–3d show diagrams of $N(\text{H})$ with respect to total reddening: the former is $N(\text{H}_2)$ derived from HCO⁺ and the latter is $N(\text{H}_2)$ derived from CO. There is a clear difference between the results of the H₂ tracers at low $N(\text{H}_2)$ and $E(\text{B} - \text{V})$. Among the fifteen HCO⁺-detected sources, three are not traced by CO. These are very likely to be dark molecular gas, and in the range of $0.07 \lesssim E(\text{B} - \text{V}) \lesssim 0.2$ or at $N(\text{H}) \lesssim 10^{21} \text{ cm}^{-2}$. It seems to be shown in panels *c–d* that, $N(\text{H})$ from HCO⁺ is systematically larger than the canonical relation (dotted line); the relation between $N(\text{H}_2)$ from HCO⁺ or CO and that from $E(\text{B} - \text{V})$ is better described by Equation (5) (dashed line), even for $E(\text{B} - \text{V}) > 0.1$ mag. Also, the distribution of $N(\text{H}_2)$ derived from HCO⁺ with respect to $E(\text{B} - \text{V})$ is less dispersed than that derived from CO. In addition, almost two-thirds of the HCO⁺-detected sources give larger molecular gas fractions ($f_{\text{H}_2} = 2N(\text{H}_2)/N(\text{H})$) than the typical value of 0.35 (e.g., Liszt et al. 2010).

Finally, our two HCO⁺-detected sources, B0838+133 and B2251+158, have similar values of $E(\text{B} - \text{V})$ (~ 0.1 mag), which are within the range shown where it is likely to be DMG. Although both are traced by CO, there is a difference between the values of $N(\text{H}_2)$ derived from HCO⁺ and CO, as shown in Table 4 and Fig. 3b. That is, the LOS of B0838+133 is expected to have additional amount of gas not traced by CO, which suggests that the LOS may contain DMG. However, DMG is not likely to exist toward B2251+158. Further studies with future observations over a larger region will uncover more details.

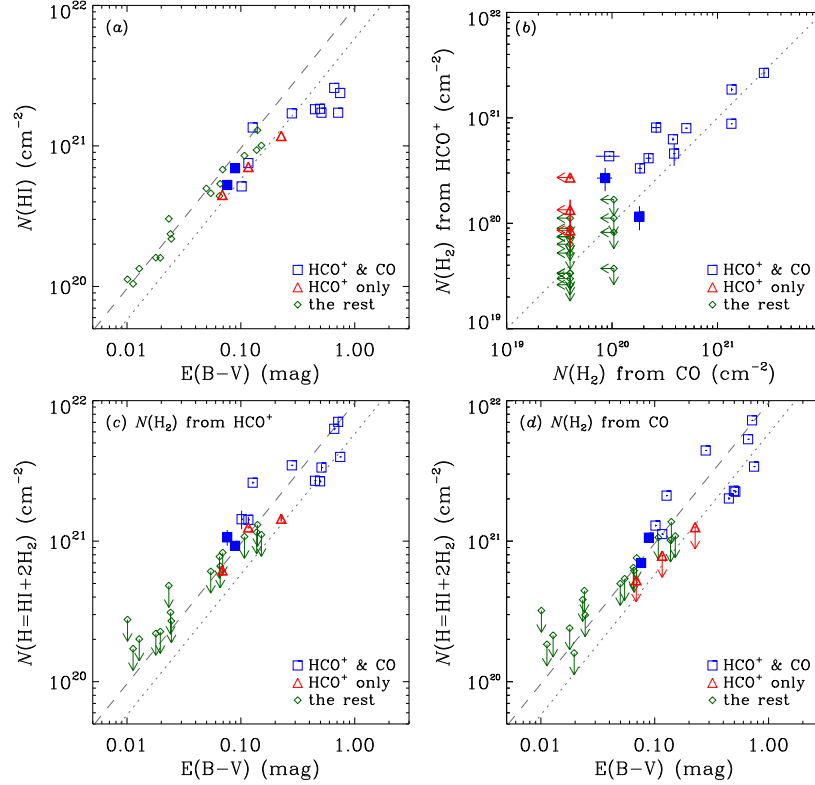


Fig. 3 (a) Column densities of atomic hydrogen vs. total reddening. Each point is calculated using data listed in Table A1 and conversion factors described in the text. Blue squares indicate sources with both HCO^+ and CO, and red triangles are sources with HCO^+ but no CO. Our two targets (B0838+133 and B2251+158) detected in the HCO^+ absorption are highlighted with a filled symbol. Green diamonds indicate the other sources without either molecules, including B2249+185 and B1228+126. Note that only the available data in the x/y-ranges of each panel are shown. The accuracy of $N(\text{HI})$ obtained from the LAB data is about 10^{19} cm^{-2} (Kalberla et al. 2005), which is negligible compared with the symbol size. The dashed line is for $N(\text{H}) = 9.65 \times 10^{21} \text{ E(B-V)} (\text{cm}^{-2}/\text{mag})$, while the dotted line is for $N(\text{H}) = 5.8 \times 10^{21} \text{ E(B-V)} (\text{cm}^{-2}/\text{mag})$. (b) Comparison of H_2 column densities derived from two different tracers. Utilized data points are same as those in (a). Errors of $N(\text{H}_2)$ from HCO^+ or CO consider only uncertainties of given observational data with fixed factors. The dotted line is where values of $N(\text{H}_2)$ from HCO^+ and CO are equal. (c) Same as (a) but total column densities of atomic and molecular hydrogen gas. $N(\text{H}_2)$ values are obtained from HCO^+ . (d) Same as (c) but $N(\text{H}_2)$ from CO.

5 Summary

We observed nine LOSs of extragalactic compact millimeter wave continuum sources in $\text{HCO}^+ J = 1 - 0$ absorption line using the KVN 21-m telescope in single dish mode. Seven of the LOSs were first observed, although B2249+185 itself was not seen during our observations. We detected HCO^+ absorption lines in two (B0838+133 and B2251+158) among the eight LOSs. The detection toward B0838+133 is a new discovery. We derived the hydrogen column densities or their limits and compared them to those inferred from CO line and far-infrared dust continuum emission. Also, we col-

lected data for other LOSs from the literature. Our main results are as follows:

(1) In the HCO^+ -undetected LOSs, CO line emission was not detected, either, and the values of E(B-V) are < 0.1 mag. The LOSs are expected to be almost entirely filled with pure atomic gas. Hydrogen column densities derived from HI line data are linearly correlated with those from the values of E(B-V) , accepting a higher conversion factor of $N(\text{H})/\text{E(B-V)} = 9.65 \times 10^{21} \text{ H} (\text{cm}^{-2}/\text{mag})$.

(2) In the two HCO^+ -detected LOSs, CO line emission was also detected and the values of E(B-V) are similar, but the differences between the values of $N(\text{H}_2)$

estimated from HCO^+ and CO line data are quite different. Our HCO^+ observational results suggest that toward B0838+133 there may be a non-negligible amount of H_2 gas not fully traced by CO, i.e., DMG. On the other hand, it is very likely that no or little DMG exists toward B2251+158.

(3) HCO^+ absorption was detected toward 15 sources at $|b| > 10^\circ$ and CO emission was not detected toward only 3 of them. The values of $E(\text{B}-\text{V})$ toward the three are 0.07–0.2 mag and, at that range, HCO^+ absorption observations could be useful to complement the missing component of molecular gas.

Acknowledgements We are grateful to the staff of the KVN who helped to operate the telescopes. The KVN is a facility operated by the KASI (Korea Astronomy and Space Science Institute). The KVN observations are supported through the high-speed network connections among the KVN sites provided by the KREONET (Korea Research Environment Open NETWORK), which is managed and operated by the KISTI (Korea Institute of Science and Technology Information).

References

- Abdo, A.A., Ackermann, M., Ajello, M., et al.: *Astrophys. J.* **710**, 133 (2010)
- Bohlin, R.C., Savage, B.D., Drake, J.F.: *Astrophys. J.* **224**, 132 (1978)
- Bolatto, A.D., Wolfire, M., Leroy, A.K.: *Annu. Rev. Astron. Astrophys.* **51**, 207 (2013)
- Fukui, Y., Okamoto, R., Kaji, R., et al.: *Astrophys. J.* **796**, 59 (2014)
- Fukui, Y., Torii, K., Onishi, T., et al.: *Astrophys. J.* **798**, 6 (2015)
- Grenier, I.A., Casandjian, J.-M., Terrier, R.: *Science* **307**, 1292 (2005)
- Heiles, C., Troland, T.H.: *Astrophys. J. Suppl. Ser.* **145**, 329 (2003)
- Kalberla, P.M.W., Burton, W.B., Hartmann, D., et al.: *Astron. Astrophys.* **440**, 775 (2005)
- Kim, K.-T., Byun, D.-Y., Je, D.-H., et al.: *Journal of Korean Astronomical Society* **44**, 81 (2011)
- Lee, S.-S., Byun, D.-Y., Oh, C. S., et al.: *Publ. Astron. Soc. Pac.* **123**, 1398 (2011)
- Li, D., Tang, N., Nguyen, H., et al.: *Astrophys. J. Suppl. Ser.* **235**, 1 (2018)
- Liszt, H.S., Wilson, R.W.: *Astrophys. J.* **403**, 663 (1993)
- Liszt, H.: *Astrophys. J.* **429**, 638 (1994)
- Liszt, H., Lucas, R.: *Astron. Astrophys.* **314**, 917 (1996)
- Liszt, H., Lucas, R.: *Astron. Astrophys.* **355**, 333 (2000)
- Liszt, H.S., Pety, J., Lucas, R.: *Astron. Astrophys.* **518**, A45 (2010)
- Liszt, H.S., Pety, J.: *Astron. Astrophys.* **541**, A58 (2012)
- Liszt, H.: *Astrophys. J.* **780**, 10 (2014)
- Lockman, F.J., Murphy, E.M., Petty-Powell, S., Urick, V.J.: *Astrophys. J. Suppl. Ser.* **140**, 331 (2002)
- Lucas, R., Liszt, H.S.: *Astron. Astrophys.* **276**, L33 (1993)
- Lucas, R., Liszt, H.: *Astron. Astrophys.* **282**, L5 (1994)
- Lucas, R., Liszt, H.: *Astron. Astrophys.* **307**, 237 (1996) (LL96)
- Miville-Deschênes, M.-A., Boulanger, F., Reach, W.T., Noriega-Crespo, A.: *Astrophys. J. Lett.* **631**, L57 (2005)
- Peek, J.E.G., Heiles, C., Putman, M.E., Douglas, K.: *Astrophys. J.* **692**, 827 (2009)
- Planck Collaboration, Ade, P.A.R., Aghanim, N., et al.: *Astron. Astrophys.* **536**, A19 (2011a)
- Planck Collaboration, Abergel, A., Ade, P.A.R., et al.: *Astron. Astrophys.* **536**, A24 (2011b)
- Planck Collaboration, Abergel, A., Ade, P.A.R., et al.: *Astron. Astrophys.* **571**, A11 (2014)
- Paradis, D., Dobashi, K., Shimoikura, T., et al.: *Astron. Astrophys.* **543**, A103 (2012)
- Savage, B.D., Bohlin, R.C., Drake, J.F., Budich, W.: *Astrophys. J.* **216**, 291 (1977)
- Savage, B.D., Mathis, J.S.: *Annu. Rev. Astron. Astrophys.* **17**, 73 (1979)
- Schlaflly, E.F., Finkbeiner, D.P.: *Astrophys. J.* **737**, 103 (2011)
- Schlegel, D.J., Finkbeiner, D.P., Davis, M.: *Astrophys. J.* **500**, 525 (1998)
- Tang, N., Li, D., Heiles, C., et al.: *Astrophys. J.* **839**, 8 (2017)
- van Dishoeck, E.F., Black, J.H.: *Astrophys. J.* **334**, 771 (1988)
- Wolfire, M.G., Hollenbach, D., McKee, C.F.: *Astrophys. J.* **716**, 1191 (2010)

A Appendix material

The data compiled in Table A1 are for sight lines of background sources at high latitudes ($|b| > 10^\circ$) listed in this paper and Table E1 of Liszt et al. (2010): total reddening ($E(B-V)$), integrated H I intensity over LSR velocities (W_{HI}), integrated optical depth of HCO^+ ($\int \tau_{\text{HCO}^+} dv$), and integrated CO intensity obtained (W_{CO}). $E(B-V)$ and W_{HI} are obtained using the same method described in Sections 4.2 and 4.1, respectively. We note that the values in Table A1 give about 14% lower values than those listed by Liszt et al. (2010), who referred to pre-update data. For $\int \tau_{\text{HCO}^+} dv$, we referred to Table 2 or to Liszt et al. (2010, and references therein). For a common line of sight between the two sets of data, the value from Table 2 was retained. And, W_{CO} values were taken from previous studies. We have adopted the values of W_{CO} provided by Liszt et al. (2010), if available. Otherwise, we have referred to the data of Liszt and Wilson (1993) or Li et al. (2018). No targets with W_{CO} from Liszt and Wilson (1993) were detected in the CO emission, so we give an upper limit assuming one Gaussian component with the peak temperature (nominal sensitivity limit; ~ 0.33 K in main beam scale) and a line width of 1.5 km s^{-1} .

Table A1 Radio Continuum Sources at $|b| > 10^\circ$ with HCO^+ Absorption Measurement

#	Source	ℓ ($^\circ$)	b ($^\circ$)	$E(B-V)$ (mag)	W_{HI} (K km s $^{-1}$)	$\int \tau_{\text{HCO}^+} dv$ (km s $^{-1}$)	W_{CO}^* (K km s $^{-1}$)
1	B1730-130	12.032	+10.812	0.4478	1002.97	1.16 \pm 0.02	0.47 \pm 0.12
2	B1908-201	16.857	-13.219	0.1376	513.53	<0.30	<0.20
3	B1741-038	21.591	+13.128	0.4955	1009.97	1.11 \pm 0.10	1.11 \pm 0.07
4	B1749+096	34.920	+17.644	0.1514	553.89	<0.14	<0.20
5	B2223-052	58.960	-48.843	0.0649	241.85	<0.45	<0.52**
6	B1663+382	61.085	+42.337	0.0101	61.79	<0.22	<0.52**
7	B1641+399	63.455	+40.948	0.0113	57.40	<0.09	<0.20
8	B2145+067	63.656	-34.072	0.0688	246.25	0.23 \pm 0.07	<0.20
9	B1954+513	85.298	+11.757	0.1270	743.34	1.68 \pm 0.06	1.89 \pm 0.04
10	B1823+568	85.739	+26.080	0.0544	252.92	<0.20	<0.20
11	B2251+158	86.111	-38.184	0.0889	381.29	0.31 \pm 0.08 [†]	0.91 \pm 0.04 [‡]
12	B2249+185	87.354	-35.648	0.0498	273.71
13	B2200+420	92.590	-10.441	0.2802	936.76	2.36 \pm 0.03	6.78 \pm 0.05
14	B1928+738	105.625	+23.541	0.1163	389.30	0.73 \pm 0.03	<0.20
15	B0212+735	128.927	+11.964	0.6608	1421.96	4.98 \pm 0.20	6.81 \pm 0.06
16	B0954+658	145.746	+43.132	0.1015	282.94	1.23 \pm 0.29	1.94 \pm 0.04
17	B0316+413	150.576	-13.261	0.1399	710.72	<0.02	<0.20
18	B0235+164	156.772	-39.108	0.0693	373.42	<0.20	<0.20
19	B0923+392	183.709	+46.165	0.0128	73.57	<0.09	<0.20
20	B0528+134	191.368	-11.012	0.7457	1307.63	2.14 \pm 0.02	2.53 \pm 0.06
21	B0420-014	195.291	-33.140	0.1075	469.05	<0.30	<0.52**
22	B0851+202	206.812	+35.821	0.0241	129.86	<0.10	<0.52**
23	B0838+133	212.968	+30.139	0.0759	289.62	0.72 \pm 0.18	0.43 \pm 0.07***
24	J0008+686	215.752	-13.253	0.7155	947.02	7.16 \pm 0.75	13.79 \pm 0.05
25	B0605-085	215.752	-13.523	0.5105	947.02	2.17 \pm 0.25	1.31 \pm 0.13
26	B0736+017	216.990	+11.380	0.1164	414.70	0.89 \pm 0.10	0.92 \pm 0.04
27	B0607-157	222.611	-16.183	0.2263	647.22	0.36 \pm 0.09	<0.20
28	B1055+018	251.513	+52.775	0.0233	166.52	<0.24	<0.20
29	B1228+126	283.778	+74.491	0.0196	87.82	<0.09	...
30	3C273	289.954	+64.360	0.0179	88.11	<0.08	<0.20
31	3C279	305.107	+57.062	0.0245	119.90	<0.07	<0.20
32	B1334-127	320.026	+48.374	0.0658	295.29	<0.17	<0.20

*Values without an alphabet letter are taken from Table E1 of Liszt et al. (2010); values with ** are from Liszt and Wilson (1993) and values with *** are from Li et al. (2018).

[†]This was reported in previous research papers of Lucas and Liszt (1996) and Liszt and Lucas (2000). The recent result gives a value of $0.280 \pm 0.005 \text{ km s}^{-1}$ using single-component Gaussian fit, which seems to be consistent with our given value within 1σ uncertainty.

[‡]Li et al. (2018) gives a slightly lower value, $W_{\text{CO}} = 0.76 \pm 0.08 \text{ K km s}^{-1}$.